Exciting Engineered Passive Dynamics in a Bipedal Robot

Daniel Renjewski, Alexander Spröwitz, Andrew Peekema, Mikhail Jones, and Jonathan Hurst

***Abstract*—A common approach in designing legged robots is to build fully actuated machines and control the machine dynamics entirely in software, carefully avoiding impacts and expending a lot of energy. However, these machines are outperformed by their human and animal counterparts. Animals achieve their impressive agility, efficiency, and robustness through a close integration of passive dynamics, implemented through mechanical components, and neural control. Robots can benefit from this same integrated approach, but a strong theoretical framework is required to design the passive dynamics of a machine and exploit them for control. For this framework, we use a bipedal spring–mass model, which has been shown to approximate the dynamics of human locomotion. This paper reports the first implementation of spring–mass walking on a bipedal robot. We present the use of template dynamics as a control objective exploiting the engineered passive spring–mass dynamics of the ATRIAS robot. The results highlight the benefits of combining passive dynamics with dynamics-based control and open up a library of spring–mass model-based control strategies for dynamic gait control of robots.**

***Index Terms*—Biologically inspired robots, force control, legged robots, motion control, passive dynamics.**

I. Introduction

Terrestrial locomotion is a fundamentally dynamic task, aiming at applying forces to the ground that are sufficient to generate support and propulsion. Given the structural complexity of animal and human legs, this task results in complex local dynamics and kinematics that make the functional understanding challenging. Scientists have discovered that, despite animals' morphological complexity, simple dynamic models can describe the fundamental principles of legged locomotion [1]–[3].

Natural locomotion, with its versatility and impressive dynamics, relies on structural compliance in legs for the physical interaction with the environment [4]. In robotics, compliance has been used to great effect for running machines [5]–[7], but rarely in walking machines. Rigid robots relying solely on their passive dynamics, inspired by the inverted pendulum model [8], are very efficient and walk dynamically but are limited to few specific walking gaits [9]–[11]. Advanced humanoids capable of versatile locomotion are fully actuated, like Asimo [12] or HRP [13], but must avoid impacts and are inherently inefficient. The well-investigated spring–mass template model for running [14]–[18] was found to also resemble the oscillatory nature of bipedal walking. It constitutes the simplest model of walking dynamics and replicates some key dynamical features of human walking [19]. On its basis, a variety of gait control strategies have been proposed [20]–[23]. Despite the theoretical potential of bipedal walking on compliant legs, few robots have actually implemented mechanical compliance [24]–[27], and none has used spring–mass dynamics as their control objective.

The bipedal robot ATRIAS (**A**ssume **T**he **R**obot **I**s **A** **S**phere) was explicitly designed to mechanically implement spring–mass model dynamics as closely as possible, combining passive dynamics with force control, in order to ultimately exploit the growing theoretical knowledge base. This approach, if implemented successfully, will allow for controller concepts from the reduced-order model to be applied to the machine, simplifying the control target from a full robot model down to one mass and two springs. Thus, for many locomotion tasks, only one control variable, the flight leg touchdown angle [28], is required. The template model controller described in this paper utilizes the robot's passive dynamics in order to enforce spring–mass dynamics by compliance matching in the leg length direction and minimizing force in the leg angle direction. We experimentally verified that the combination of 1) intentionally designed passive dynamics and 2) control enforcing desired dynamics utilizing the robot's passive compliance can maintain a walking gait like that predicted by the model.

The contribution of this paper is twofold: 1) demonstrating, for the first time, a spring–mass walking gait on robotic hardware; and 2) the application of a dynamics-based control objective originating from a reduced-order dynamic template to generate dynamic locomotion in a machine.

II. Methods

In our experiments, we tested the robot in a controlled experimental setup for its capabilities to utilize its natural leg compliance to match spring–mass model walking dynamics.

A. Template Model Simulation

The spring–mass model is the simplest dynamic template for human walking. In this numerical simulation, the entire mass of a walker is lumped into a point, and the interaction with the ground is governed by a massless elastic leg exerting forces

Manuscript received October 27, 2014; revised April 20, 2015; accepted August 21, 2015. Date of publication September 16, 2015; date of current version September 30, 2015. This paper was recommended for publication by Associate Editor C. Ott and Editor A. Kheddar upon evaluation of the reviewers' comments. This work was supported by the Defense Advanced Research Projects Agency under Grant #W91CRB-11-1-0002, the Human Frontier Science Program under Grant #RGY0062/2010, and the National Science Foundation under Grant #1100232.

D. Renjewski is with the Robotics and Embedded Systems Group, Technische Universität München, 85748 Garching, Germany (e-mail: daniel.renjewski@tum.de).

A. Spröwitz is with the Physical Intelligence Department, Max Planck Institute for Intelligent Systems, 70569 Stuttgart, Germany (e-mail: sprowitz@is.mpg.de).

A. Peekema, M. Jones, and J. Hurst are with the Dynamic Robotics Laboratory, School of Mechanical, Industrial and Manufacturing Engineering, Oregon State University, Corvallis, OR 97331 USA (e-mail: peekemaa@onid.orst.edu; jonesmik@engr.orst.edu; jonathan.hurst@oregonstate.edu)

This paper has supplementary videos and experimental data that are available at http://daniel.human-motion-engineering.org/ATRIAS

Color versions of one or more of the figures in this paper are available online at http://ieeexplore.ieee.org.

Digital Object Identifier 10.1109/TRO.2015.2473456

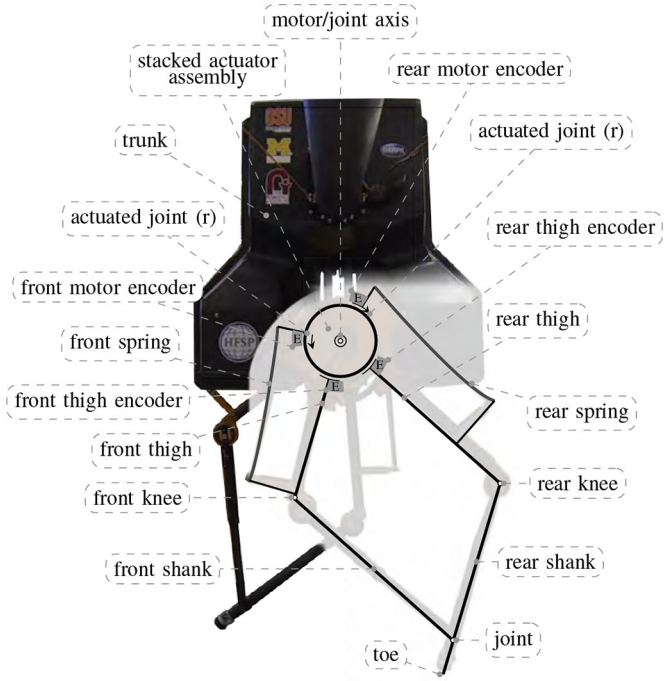

Fig. 1. Topology and key technical features of the ATRIAS robot. A stacked motor assembly houses two motors with harmonic drives sharing one axis of rotation with the front and rear thighs and independently driving the proximal end of front and rear spring, respectively. Optical encoders (E) with a 32-bit resolution measure the displacement of all four segments around the hip, thus allowing for accurate measurement of spring deflection. Rear and front thigh are joined by rear and front shank to form a four-bar mechanism allowing for accurate force control (see Fig. 3). The trunk houses an additional actuated degree of freedom for each leg (not indicated) allowing its abduction. Furthermore power electronics, batteries and control computer are located inside the trunk.

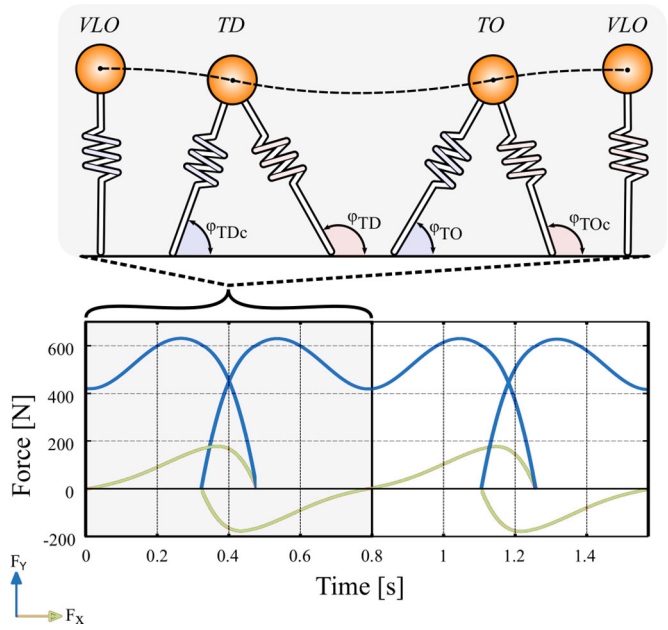

Fig. 2. Walking limit cycle: VLO in single support, touchdown (TD) into double support, and takeoff (TO) back to single support. Gait trigger angles for the robot are indicated on their corresponding state figures ($\varphi_{\mathrm{TD}}, \varphi_{\mathrm{TO}c}, \varphi_{\mathrm{TD}c}, \varphi_{\mathrm{TO}}$), where φ_{TD} is the touchdown angle, $\varphi_{\mathrm{TO}c}$ is the stance leg angle at the start of single support, $\varphi_{\mathrm{TD}c}$ is the stance leg angle when the flight leg touches down, and φ_{TO} is the leg angle the instant before flight. The plot shows the ideal forces experienced by each leg through one cycle of VLO to VLO for the gait that was experimentally tested.

to the point mass and the contact point on the ground. The spring–mass model for walking is fully defined by four state variables, which are the center of mass position and velocity $[x, y, \dot{x}, \dot{y}]$ and three parameters (mass m, leg length l_0, and spring stiffness k). The control variable to achieve steady-state walking is the touchdown angle (φ_{TD}). The spring–mass model is able to reproduce the general characteristics of experimentally observed ground reaction forces (see [19], Fig. 2).

The proposed control strategies allow the model, for instance, to balance an extended upper body [21]. In this study, we focus on implementing the basic sagittal plane walking dynamics of the spring–mass model on even terrain.

Equations of motion can be derived using Newtonian methods:

$$m\ddot{x} = F_x \tag{1}$$

$$m(\ddot{y} + g) = F_y \tag{2}$$

where F_x and F_y are a projection of spring forces. If there are two legs on the ground, they both contribute to these forces; with one leg on the ground, the swing leg does not contribute forces as it is massless. Due to the robot's leg geometry, the spring force is nonlinear with respect to leg deflection. The expected nonlinear force is derived using a static analysis of the ATRIAS leg and yields the following equation for the leg force in the axial direction:

$$F_{\mathrm{ax}}(l) = \frac{2 * \kappa * (a\cos(l_0) - a\cos(l))}{\sqrt{(1 - l^2)}} \tag{3}$$

where κ is the rotational stiffness of the physical springs, l_0 is the leg's resting length, and l is the current leg length.

The equations of motion are implemented in MATLAB (2013b, The Mathworks, Natick, MA, USA) and numerically integrated using *ode45* (rel. and abs. tolerance 1e-8). The simulation begins at apex and vertical leg orientation (VLO) and a positive forward velocity (see Fig. 2). The initial state and control variable are chosen to match the robot's operation range, and one cycle consisting of single support, double support, and single support is simulated. The touchdown angle is optimized using *fminsearch* to yield a limit cycle, i.e., the state where the terminal apex matches the initial conditions. Stance leg angles during phase transitions are recorded as trigger points for the robot controller (see Fig. 2).

The gait simulated for experiments had a VLO state of $x = 0\,\mathrm{m}, y = 0.870\,\mathrm{m}, \dot{x} = 0.763\,\mathrm{m/s}, \dot{y} = 0\,\mathrm{m/s}$, control angles of $\varphi_{\mathrm{TD}} = 1.144\,\mathrm{rad}, \varphi_{\mathrm{TO}c} = 1.297\,\mathrm{rad}, \varphi_{\mathrm{TD}c} = 1.845\,\mathrm{rad}, \varphi_{\mathrm{TO}} = 1.998\,\mathrm{rad}$, and a resting leg length of $0.9\,\mathrm{m}$. This gait has a duty cycle of 0.59 and a peak vertical force of $630\,\mathrm{N}$ (see Fig. 2).

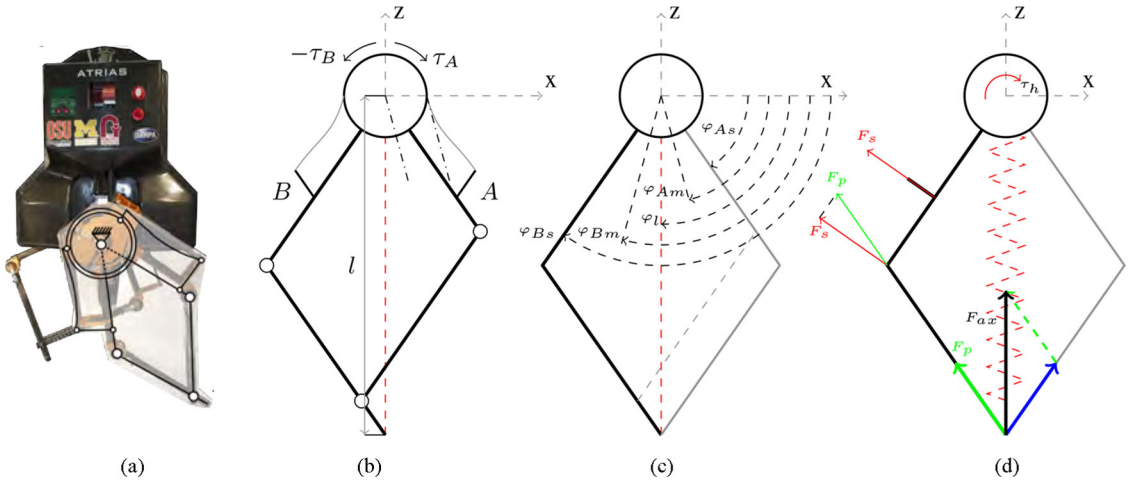

Fig. 3. Schematic representation of *ATRIAS*' leg geometry, and force transmission. (a) Schematic abstraction of the mechanical leg design: (b) Four-bar leg mechanism (thick lines) and attached springs (thin lines) connected to their respective motors A and B. Dash-dotted lines indicate the angle at the motor output projected to the hip joint. The virtual leg is indicated by the vertical dashed line. (c) Angle definitions: φ_{As}—side A segment angle, φ_{Am}—side A motor angle, φ_l—virtual leg angle, φ_{Bs}—side B segment angle, φ_{Bm}—side B motor angle. (d) Force projection: F_s—spring reaction force on spring attachment and projected onto joint, F_p—spring reaction force projected on lower segment, F_{ax}—reaction force along leg axis resulting from spring deflections of spring A and spring B. The assumed virtual leg spring is depicted as a dashed line.

B. Robot Background

All experiments were executed on the bipedal robot *ATRIAS* (see Fig. 1), a machine of 1.70-m height and 60-kg weight. The mass of the robot is concentrated in the trunk, one leg accounts for about 5% of the total weight. Six motors power the robot: two in parallel on each leg driving the leg in the sagittal plane and one for leg abduction in the frontal plane. The *ATRIAS* robot neglects the morphology of biological legs to implement the dynamic functionality of a compliant leg as proposed by the bipedal spring–mass model. A four-bar mechanism gears the dynamic interaction between a pair of series elastic actuators (SEAs) and the supporting substrate (see Fig. 3). A symmetric force application through both physical springs results in a force purely along the leg axis, because tangential force components cancel each other out (Table I).

A virtual spring connecting the toe and the hip is assumed to match the spring–mass model topology [see Fig. 3(d)]. Although the physical springs of the SEAs have a nearly linear torque–angle relation (κ, 1600 N·m/rad), the linkage system induces a virtual nonlinear degressive spring stiffness for the entire leg [k, Eq. (3)]. The robot's CoM is located approximately 12 cm above the hip joint and, for the small weight of the segments in motion, does not move much itself. At the same time, the controller aims at minimizing hip torques, and thus, only small torques act on the CoM, because the lever for the leg forces is small. Therefore, the hip position is a good representation of the CoM, and the virtual leg connecting hip and CoP and the axial forces correspond to the respective properties of the spring–mass model.

Like any other physical system, this robot did not operate in an energy conserving manner. Mechanical energy has been dissipated, for example, through friction and nonelastic collisions and must be replenished through controlled actuation.

C. Robot Technical Specifications

As much as possible commercially available components were used in the ATRIAS design. The motors attached to each spring (MF0150010-X0X, Allied Motor Technologies, Tulsa, OK, USA) are rated for 532-W continuous power, geared with a 50:1 harmonic drive (CSD-50-50-2A-GR-BB-SP3336, Harmonic Drive LLC, Peabody, MA, USA) and deliver a theoretical stall torque of 300 N·m at the gear output end. Four 32-bit optical encoders (RL32BAT001B30F, Renishaw, Wotton-under-Edge, U.K.) measure the motor positions φ_{Am} and φ_{Bm} and the segment positions φ_{As} and φ_{Bs} relative to the trunk's anteroposterior axis [see Figs. 1 and 3(c)].

The trunk houses two motors for leg abduction (QB02303-X0X-H, Allied Motor Technologies, Tulsa, OK, USA) that drive pulley segments on large lever arms giving a 56:1 gear ratio. Power and control electronics positioned in the lower trunk are wired using an *Ethercat*-bus architecture into the on-board main control computer (Mini ITX, i1000A, OEM Production, San Francisco, CA, USA). Controllers have been implemented in *C++* and were executed at a 1-kHz control rate. Control parameters were altered remotely using a graphical user interface. Specifications of the software architecture are given in [29].

The four-bar mechanism is composed of carbon-fiber tubes connected by aluminum joints. The ground contact is made by a spherical rubber knob at the toe.

D. Experimental Setup

For all experiments, the ground was covered with stiff rubber mats to avoid slipping of the toe. The boom was firmly attached to the trunk and locked trunk pitch. Encoders on the boom measured the robot's horizontal and vertical displacement. To minimize unintended interference during the experiments, the

TABLE I
DERIVED KINEMATIC AND DYNAMIC ROBOT STATES

Virtual leg angle	$\varphi_l = \frac{\varphi_{Bl} + \varphi_{Al}}{2}$
Virtual leg length	$l = 2 \cdot s \cdot \cos(\varphi_l - \varphi_{Al})$
Spring deflection A	$\varphi_{As} = \varphi_{Am} - \varphi_{Al}$
Spring deflection B	$\varphi_{Bs} = \varphi_{Bm} - \varphi_{Bl}$
Leg spring stiffness	$k = \frac{\kappa}{2s^2}\left(\frac{\chi - \frac{l}{2s}\cdot\left(a\cos\left(\frac{l}{2s}\right) - a\cos\left(\frac{l_0}{2s}\right)\right)}{\chi^3}\right)$
	$\chi = \sqrt{\left(1 - \left(\frac{l}{2s}\right)^2\right)}$
Axial leg force	$F_{\mathrm{ax}}(\varphi) = \frac{\kappa}{2s}\cdot\left(\frac{\varphi_{Am}}{\sin(\varphi_{As} - \varphi_l)} + \frac{\varphi_{Bm}}{\sin(\varphi_l - \varphi_{Bs})}\right)$
Hip torque	$\tau_h = \tau_A + \tau_B$
Tangential leg force	$F_{\tan} = \tau_h \cdot l$

boom was designed with low rotational inertia and friction (see Fig. 4).

E. Template Model-Based Control

While walking, the robot constitutes a hybrid dynamical system. From the perspective of a single leg, there are two dynamically distinct phases: stance and swing. Accordingly, walking control for each leg is broken up into stance and swing. The spring–mass template model provides the desired stance force profile. This is translated to a command to apply purely axial force based on the current leg length and physical spring stiffness, thus matching the natural leg stiffness. This force is used as the feedforward term, and deviations are compensated with a PD feedback controller, with the proportional gain being set to 500 A/N and the derivative gain being 50 A·s/N (see Fig. 5). Gains were set manually to achieve good tracking while avoiding oscillations.

Unlike the robot, the template model does not require a flight controller as the leg is massless. Flight control objectives are to provide ground clearance, fast takeoff, smooth touchdown, and timely leg recirculation considering motor constraints. We formulated a cubic spline that describes the toe trajectory in terms of leg length and leg angle to protract the leg in order to satisfy all of these constraints (see the Appendix for equation and Fig. 6 for the resulting trajectory).

Switching between swing and stance control is triggered based on stance leg angles derived from simulation (φ_{TD}, $\varphi_{\mathrm{TD}c}$, $\varphi_{\mathrm{TO}c}$, and φ_{TO}; see Fig. 2). Each leg's stance phase is divided into three phases defined by the four angles: first double support, then single support, and finally, double support. The swing phase occurs during the single support of the other leg. This phase timing implicitly dictates the model predicted duty cycle, i.e., the ratio of stance time to cycle time.

F. Data Processing

Sensor data of the robot have been recorded and processed for use in MATLAB (2012b, The Mathworks, Natick, MA, USA).

Fig. 4. Experimental setup: robot mounted to the boom, graphical user interface visible in the top left corner. When operating, the robot was always carrying its own weight. The suspension cord only acted as a fail-safe and was carefully adjusted to stay slack during experimental operation.

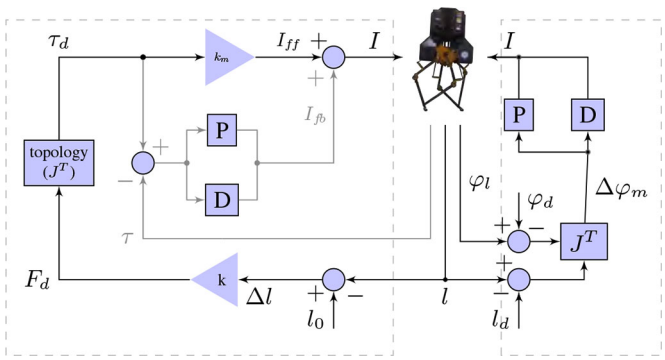

Fig. 5. *Stance leg controller (left side)*: Based on the current leg length (l), the respective force (F_d) of the virtual leg spring is calculated and translated into desired motor torques (τ_d). By multiplication with the motor constant (k_m), a feedforward current (I_{ff}) is commanded (black feedforward loop). Through measuring the spring deflection, the actual torque (τ) is determined and deviations from the desired torque are corrected through a PD control loop (gray feedback loop). The resulting sum of currents (I) is sent to the robot's amplifiers. *Flight leg controller (right side)*: Deviation of the flight leg (l, φ_l) from the desired trajectory (l_d, φ_d) is translated into motor position deviation ($\Delta\varphi_m$) and regulated by a PD controller.

Electrical and mechanical power and cost of transport (CoT) were calculated from experimental data. Sensors measured the current (HASS 50-S, LEM USA Inc., Milwaukee, WI, USA) through the robot's power supply cables and the supply voltage. The voltage signal was filtered using a single-pole recursive low-pass filter. The mean over the trial for both current and voltage was calculated. The electrical power results in

$$P_{\mathrm{el}} = \tilde{U} \cdot \tilde{I} \tag{4}$$

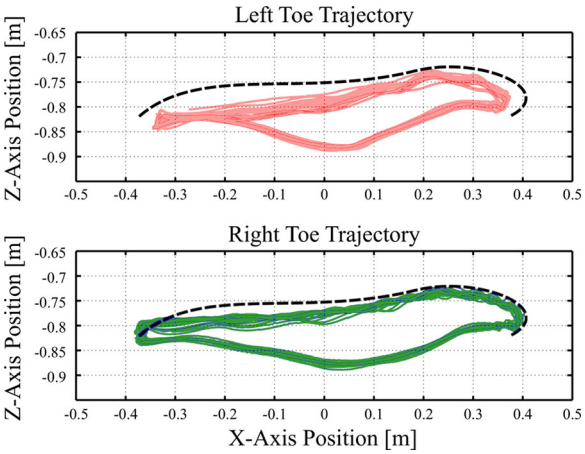

Fig. 6. Measured toe trajectory of left (top) and right (bottom) leg relative to the robot's trunk. The dashed black line indicates the desired swing phase trajectory. Deviations for the most part result from the circular path of the robot.

where $\tilde{U}$ and $\tilde{I}$ denote the average voltage and current over the trial, respectively. The electrical CoT is defined as

$$\mathrm{CoT}_{el} = \frac{P_{el}}{m \cdot g \cdot \tilde{v}} \tag{5}$$

with m being the robot's mass, g being the gravitational acceleration, and $\tilde{v}$ being the forward velocity averaged over a number of full gait cycles. The mechanical power generated for forward locomotion was derived from the calculated leg forces (F) and instantaneous velocity (v)

$$P_{\text{mech}} = \frac{1}{\sigma} \sum_{i=1}^{\sigma} F_i \cdot v_i \tag{6}$$

with σ denoting the number of samples in a trial. The mechanical CoT was calculated accordingly

$$CoT_{\text{mech}} = \frac{P_{\text{mech}}}{m \cdot g \cdot \tilde{v}}. \tag{7}$$

For better comparison, the Froude number, a dimensionless characteristic velocity, was calculated as

$$F_r = \frac{\tilde{v}^2}{g \cdot l_0}. \tag{8}$$

In order to determine the mechanical energy of the robot, potential and kinetic energy has been summed

$$\begin{aligned} E &= E_{\text{pot}} + E_{\text{kin}} + E\text{spring} \\ &= mgy + \frac{1}{2}mv^2 + \frac{1}{2}\kappa(\varphi_{As}^2 + \varphi_{Bs}^2). \end{aligned} \tag{9}$$

The energy stored in the nonlinear leg spring has been calculated numerically as

$$E_{\text{spring}}^{l} = \int_{l=l_0}^{l_{\min}} F_{\text{ax}} dl. \tag{10}$$

In order to compare the passive and active contributions of leg force generation, the power contributions of motors and spring in the leg length direction were calculated. In order to isolate the axial power, generated hip torques and the velocity of leg retraction during stance were neglected. For the motors, we subtracted the angular velocity of the leg from each motor velocity and multiplied by the generated symmetric torque

$$\begin{aligned} P_{\text{motor},ax} = &(\dot{\varphi}_{Am} - \dot{\varphi}_l) \cdot \min(|\tau_A|, |\tau_B|) \cdot \text{sign}(\tau_A) \\ &+ (\dot{\varphi}_{Bm} - \dot{\varphi}_l) \cdot \min(|\tau_A|, |\tau_B|) \cdot \text{sign}(\tau_B). \end{aligned} \tag{11}$$

The generated symmetric torque is calculated as the minimum of the instantaneous torque generated by both springs. The springs' power contributions are calculated from the symmetric spring deflection velocity multiplied by the generated symmetric torque

$$\begin{aligned} P_{\text{spring}} = &\text{sign}(\dot{\varphi}_{As} - \dot{\varphi}_{Am}) \\ &\cdot \min(|\dot{\varphi}_{As} - \dot{\varphi}_{Am}|, |\dot{\varphi}_{Bs} - \dot{\varphi}_{Bm}|) \\ &\cdot \min(|\tau_A|, |\tau_B|) \cdot \text{sign}(\tau_A) \\ &+ \text{sign}(\dot{\varphi}_{Bs} - \dot{\varphi}_{Bm}) \\ &\cdot \min(|\dot{\varphi}_{As} - \dot{\varphi}_{Am}|, |\dot{\varphi}_{Bs} - \dot{\varphi}_{Bm}|) \\ &\cdot \min(|\tau_A|, |\tau_B|) \cdot \text{sign}(\tau_B). \end{aligned} \tag{12}$$

The spring velocity is calculated as the velocity differential between both ends of the springs. The symmetric spring velocity is calculated as the instantaneous minimum of both spring velocities of one leg.

III. Results

Body support and propulsion was consistently achieved; leg recirculation resulted in smooth transitions from stance into swing and back. Although the robot did not explicitly sense ground contact, the compliant leg allowed for soft touchdown (see Fig. 6). ATRIAS was able to walk successfully in repeated trials and reproduced the dynamics of the template model for human walking, matching the energy fluctuations observed in the simulation model (see Fig. 7). The reported data have been taken from a single experiment, 12 steps of which were averaged. Fig. 8 shows the measured ground reaction forces of the robot in comparison with the targeted model dynamics. The robot dynamics match the targeted dynamics very well; force magnitude and directions deviate insubstantially. Forces perpendicular to the leg account for less than 10% of the overall force. Therefore, the deviation of force direction and leg axis ($\Delta\varphi$) is small.

Energy fluctuation as observed in the experiment shows the same magnitude as predicted by the model (see Table II), indicating that about the same amount of mechanical energy predicted by the simulation model has been stored in the physical springs of the robot. The phase shift of energy fluctuation (see Fig. 8) results from a slight mismatch of cycle times.

The magnitude of vertical forces is comparable (630 N in the model, 640 N in the experiments), although the second hump in the experiment is smaller than the first. In concert with the shifted horizontal ground reaction force, this can be attributed to dissipation in the robot. The robot is slowing down over the duration of the experiment as visible in the asymmetry of the horizontal impulse and was gently pushed to keep it moving.

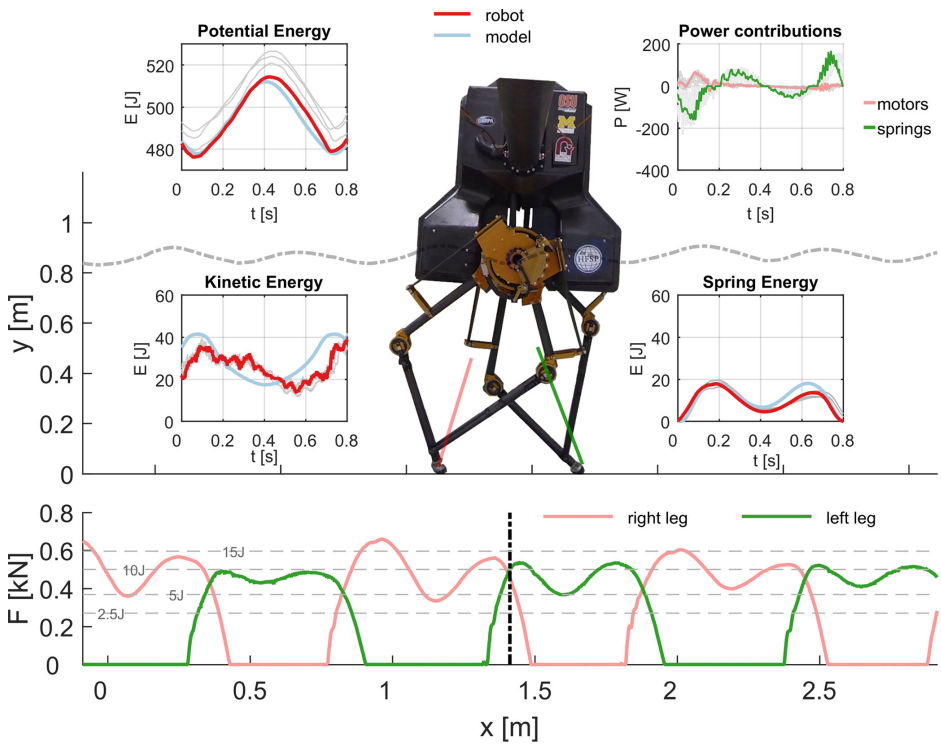

Fig. 7. Visualization of experimental results. The circulation of energy through compliant elements that governs the template dynamics and accounts for efficiency is a main property we aim at reproducing in the robot. The top panel shows the CoM trajectory of the walking ATRIAS robot during the experiments. Three inline plots show the fluctuation of gravitational, kinetic, and elastic energies over one stance phase; the top right plot shows the respective power contributions of springs and motors over stance, respectively. In each energy plot, one exemplary experimental cycle is highlighted (dark bold line) and compared with the respective energy curve of the computational model (bright bold line). The inline figure labeled "spring energy" compares the energy stored in the passive springs of the robot during the experiment over one stance phase with the energy stored in the leg spring of the simulation model. Magnitudes indicate a substantial storage and release of CoM energy by the springs. Power contributions indicate that substantial power is absorbed and regenerated by the springs, while the motor contribute only a fraction to the leg axis power. The bottom panel shows the experimentally determined leg force of the robot, dashed lines indicate corresponding levels of energy stored in the virtual leg spring. The resemblance of the model forces (see Fig. 2) illustrates the close dynamic matching of the model for animal gait and the robot, driven by leg elasticity for energy recycling.

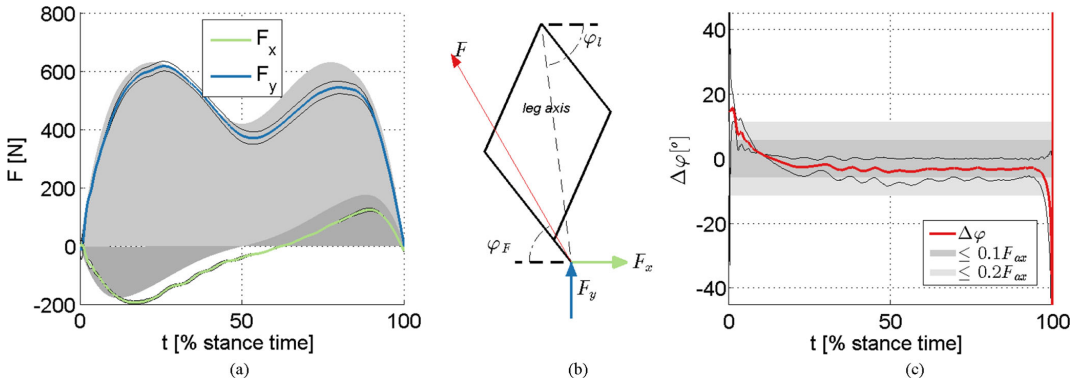

Fig. 8. (a) Comparison of Cartesian ground reaction forces from simulation (gray area) and experiment (bold line). As ground reaction forces substantiate global dynamics, the matching forces are indicative of the robot matching the desired dynamics. (b) Schematic illustrating force definitions and the deviation between leg axis and leg force. (c) Deviation of the leg force from the leg axis during stance phase is indicated. Zero degree corresponds to no deviation; the dark and light gray areas correspond to a tangential force amounting to 10% and 20% of total leg force, respectively. For most part of the gait cycle, less than 10% of the total leg force are not axial further confirming the successful dynamic matching.

Stance duration has been predicted by the model to be 0.78 s and turned out as 0.83 $\pm$ 0.02 s in the experiment. The average speed of the robot has been 0.85m/s resulting in a Froude number of 0.08, while the model predicted a velocity of 0.95 m/s. This deviation is most certainly a result of the energy loss in the robot.

The electrical power consumption was measured to be 550W resulting in an electrical CoT of 1.1. The mechanical CoT is 0.2 at a mechanical power consumption of 105W [30].

The measured angle of attack of the robot averaged to 1.17 $\pm$ 0.00 rad and matched the intended angle of 1.14 rad closely, deviating only 1.8%.

TABLE II
ENERGY FLUCTUATIONS IN SIMULATION MODEL AND ROBOT EXPERIMENT

	model		robot	
energy	min	max	min	max
kinetic	17.5 J	41.5 J	13.9 ± 3.0 J	39.9 ± 2.4 J
spring	0 J	18.2 J	0 J	18.2 ± 1.3 J

As clearly visible in Fig. 7, energy and ground reaction forces cycle consistently, indicating the robot's ability to match a stable gait over a number of steps. The commonly reported apex state $[\dot{x}, y]$ for assessing dynamic gait stability showed only minor fluctuations ($[0.77 \pm 0.06\,\text{m/s}, 0.89 \pm 0.02\,\text{m}]$) and matched the model prediction of $[0.76\,\text{m/s}, 0.87\,\text{m}]$.

The power contributions in leg axis direction as depicted in Fig. 7 indicate a substantial contribution by the robots passive compliant elements. The motors generate positive power mainly during impact absorption in the first quarter of stance.

IV. DISCUSSION

In dynamic locomotion, kinematics are a result of meaningful dynamics rather than a control objective in themselves. The presented approach uses dynamics predicted by a template model for gait as the control objective. The hardware design that incorporates desired passive dynamics and the ability to control global dynamics are necessary requirements for template-based control. This approach is significantly different from other control methods for bipedal robots.

Few actuators have sufficient bandwidth to actively control compliance in order to generate the dynamics observed in bipedal locomotion. However, the ability to mimic passive dynamics with active compliance control comes at a high cost of required power. Passive elements amplify actuator power and thus relax the requirements for active components. This is obvious when looking into the power contributions of active and passive elements during our experiment (see Fig. 7, top right panel). As ATRIAS' leg has a second degree of freedom and actuators need to actively follow the leg retraction during stance, partially against the generated spring torques, the motors contribute substantially more power to the rotational degree of freedom.

The successful mechanical implementation of a biologically relevant template model in a full-size bipedal robot marks a milestone in dynamic robotics developments. In our experiments, we were able to demonstrate that the passive compliance of the robot can be combined with actuation in a meaningful way to facilitate sustainable, dynamic locomotion by matching a dynamic template. To our knowledge, this is the first time that spring–mass bipedal walking has been implemented. The reproduction of typical ground reaction forces observed in the spring–mass model for walking indicates the dynamic match of model and robot. This achievement lays the foundation for the application of control concepts proposed by studies of the spring–mass model to negotiate different kinds of terrain, over a range of speeds, while limiting structural dynamic loads. The ability of ATRIAS to modulate the leg force, e.g., by adding hip torques through asymmetric spring torques allows for expanding the current control approach in order to stabilize the upper body and to regulate momentum and energy.

This demonstration of the robot's dynamics reproduced a number of model predictions. Force amplitudes and trajectories as well as stride time have been well matched, and the achieved mechanical CoT of 0.2 and electrical CoT of 1.1 indicate a high potential for efficient locomotion, advertising the use of compliant structures that allow for kinetic and gravitational energy to be stored and recycled. For reference, human walking is reported to have a CoT of 0.05 (mech.) and 0.2 (metabolic). For robots, the CoT spans a range from 0.055 (mech.) and 0.2 (elec.) for the Cornell Ranger to estimated 1.6 (mech.) and 3.2 (elec.) for Honda's ASIMO [11]. A recent study on energy optimized ZMP walking reported an electrical CoT as high as 4.7 [31]. While energy efficiency is one of the key factors required for mobile machines, as they have to carry their source of energy, different levels of autonomy, versatility, and performance make it hard to directly compare robots.

In general, we found that compliant legs remove the need to actively control the impact in order to avoid structural damage to the robot and, therefore, largely relaxes control and improves robustness. Passive elements with well-known properties additionally serve as accurate force sensors.

A. Scientific Impact

Template models like the spring–mass model are often used to discover basic principles in animal locomotion [2], [4]. The declaratory nature of model findings not tested in the real world has been criticized in [32]. While the inverted pendulum concept has found its real-world representation in a number of robots, few technical devices were engineered to reproduce spring–mass dynamics for bipedal walking, leaving existing theoretical work in the realm of simulation. This approach enables the implementation of control strategies discovered in experimental studies and through investigating template models such as leg force-limiting in obstacle negotiation [33], virtual pivot-point control for trunk stabilization [21], and bipedal locomotion in three dimensions [18], [23]. The successful implementation of, and continued experimentation with, bioinspired dynamics will lead to a better understanding how the interplay of mechanics and neural control allows animals to achieve the performance we observe.

V. CONCLUSION

Evidence strongly suggests that the spring–mass behavior is general to legged locomotion. We suggest that further expansion of this concept of integrated design and control, which embraces passive dynamics and active control, has the potential to enhance legged robots to ultimately match the efficiency, agility, and robustness of animals over a variety of terrain. The integrated design approach that embraced the template-based control objective presented in this paper allows for the first time the implementation of spring–mass model dynamics of walking

in a human-size bipedal robot, achieving efficient and dynamic walking.

APPENDIX
SWING CONTROLLER

The progression of the swing leg on the flight trajectory is driven by the motion of the stance leg through a predefined range $[\varphi_{\mathrm{TO}c}, \varphi_{\mathrm{TD}c}]$ mapped to $[x_1, x_2]$. Boundary conditions ($[y_1, \dot{y}_1], [y_2, \dot{y}_2]$) shape the spline. The general formulation is described by the following equations:

$$\begin{aligned}
a_0 &= 2*(y_1 - y_2) + (\dot{y}_1 + \dot{y}_2)*(x_2 - x_1) \\
a_1 &= y_2 - y_1 - \dot{y}_1*(x_2 - x_1) - a_0 \\
a_2 &= \dot{y}_1*(x_2 - x_1) \\
a_3 &= y_1 \\
s &= (x - x_1)/(x_2 - x_1) \\
y &= a_0*s^3 + a_1*s^2 + a_2*s + a_3 \\
\dot{y} &= \dot{x}*\left[-3*\frac{a_0*(x-x_1)^2}{(x_1-x_2)^3} + 2*\frac{a_1*(x-x_1)}{(x_1-x_2)^2} \right. \\
&\quad \left. -\frac{a_2}{(x_1-x_2)}\right]. \qquad (13)
\end{aligned}$$

ACKNOWLEDGMENT

The authors would like to thank K. Morton, R. van Why, M. Anderson, S.-H. Yoo, and R. Skeele for their respective contributions to the robot's control and data acquisition system and their support to execute the experiments.

REFERENCES

[1] R. Blickhan, "The spring-mass model for running and hopping," *J. Biomech.*, vol. 22, no. 11-12, pp. 1217–1227, 1989.
[2] R. J. Full and D. E. Koditschek, " Templates and anchors: Neuromechanical hypotheses of legged locomotion on land," *J. Exp. Biol.*, vol. 202, no. 23, pp. 3325–3332, 1999.
[3] H. Geyer, A. Seyfarth, and R. Blickhan, "Compliant leg behaviour explains basic dynamics of walking and running," *Proc. Roy. Soc. B Biol. Sci.*, vol. 273, no. 1603, pp. 2861–2867, 2006.
[4] R. Blickhan, A. Seyfarth, H. Geyer, S. Grimmer, H. Wagner, and M. Günther, "Intelligence by mechanics," *Philosoph. Trans. Roy. Soc. A, Math. Phys. Eng. Sci.*, vol. 365, no. 1850, pp. 199–220, 2007.
[5] M. H. Raibert, *Legged Robots that Balance*, vol. 3. Cambridge, MA, USA: MIT Press, 1986.
[6] M. H. Raibert, "Legged robots," *Commun. ACM*, vol. 29, no. 6, pp. 499–514, 1986.
[7] M. Ahmadi and M. Buehler, "Controlled passive dynamic running experiments with the ARL-monopod II," *IEEE Trans. Robot.*, vol. 22, no. 5, pp. 974–986, Oct. 2006.
[8] M. Garcia, A. Chatterjee, A. Ruina, and M. Coleman, "The simplest walking model: Stability, complexity, and scaling," *J. Biomech. Engng.*, vol. 120, pp. 281–288, 1998.
[9] T. McGeer, "Passive dynamic walking," *Int. J. Robot. Res.*, vol. 9, pp. 62–82, 1990.
[10] S. H. Collins, "A three-dimensional passive-dynamic walking robot with two legs and knees," *Int. J. Robot. Res.*, vol. 20, no. 7, pp. 607–615, 2001.
[11] S. Collins, A. Ruina, R. Tedrake, and M. Wisse, "Efficient bipedal robots based on passive-dynamic walkers," *Science*, vol. 307, pp. 1082–1085, 2005.
[12] S. Kazuo, K. Tsuchiya, and K. Tsujita, "The intelligent ASIMO system overview and integration," in *Proc. Int. Conf. Robot. Autom.*, New Orleans, LA, USA, 2004, pp. 3043–3048.
[13] K. Kaneko, F. Kanehiro, M. Morisawa, K. Akachi, G. Miyamori, A. Hayashi, and N. Kanehira, "Humanoid robot hrp-4-humanoid robotics platform with lightweight and slim body," in *Proc. IEEE/RSJ Int. Conf. Intell. Robots Syst.*, 2011, pp. 4400–4407.
[14] J. Schmitt and P. Holmes, "Mechanical models for insect locomotion: Dynamics and stability in the horizontal plane-ii. Application," *Biol. Cybern.*, vol. 83, no. 6, pp. 517–527, 2000.
[15] P. Holmes, R. J. Full, D. Koditschek, and J. Guckenheimer, "The dynamics of legged locomotion: Models, analyses, and challenges," *Siam Rev.*, vol. 48, no. 2, pp. 207–304, 2006.
[16] I. Poulakakis and J. Grizzle, "The spring loaded inverted pendulum as the hybrid zero dynamics of an asymmetric hopper," *IEEE Trans. Autom. Control*, vol. 54, no. 8, pp. 1779–1793, Aug. 2009.
[17] R. Altendorfer, U. Saranli, H. Komsuoglu, D. E. Koditschek, B. Brown, M. Buehler, E. Moore, D. McMordie, and R. J. Full, "Evidence for spring loaded inverted pendulum running in a hexapod robot," in *Experimental Robotics VII*. New York, NY, USA: Springer, 2002.
[18] H.-M. Maus and A. Seyfarth, " Walking in circles: A modelling approach," *J. R. Soc. Interface*, vol. 11, no. 99, p. 20140594, 2014.
[19] S. W. Lipfert, M. Günther, D. Renjewski, S. Grimmer, and A. Seyfarth, "A model-experiment comparison of system dynamics for human walking and running," *J. Theor. Biol.*, vol. 292, pp. 11–17, 2012.
[20] Y. Blum, S. W. Lipfert, J. Rummel, and A. Seyfarth, "Swing leg control in human running," *Bioinspiration Biomimetics*, vol. 5, no. 2, p. 026006, 2010.
[21] H.-M. Maus, S. W. Lipfert, M. Gross, J. Rummel, and A. Seyfarth, "Upright human gait did not provide a major mechanical challenge for our ancestors," *Nature Commun.*, vol. 1, no. 6, p. 70, Jan. 2010.
[22] C. Hubicki and J. W. Hurst, "Running on soft ground: Simple, energy-optimal disturbance rejection," in *Proc. 5th Int. Conf. Climbing Walking Robots Support Technol. Mobile Mach.*, 2012, pp. 543–547.
[23] F. Peuker, C. Maufroy, and A. Seyfarth, "Leg-adjustment strategies for stable running in three dimensions," *Bioinspiration Biomimetics*, vol. 7, no. 3, p. 036002, 2012.
[24] S. Hyon and T. Emura, "Symmetric walking control: Invariance and global stability," in *Proc. IEEE Int. Conf. Robot. Autom.*, 2005, pp. 1443–1450.
[25] R. Niiyama, S. Nishikawa, and Y. Kuniyoshi, "Athlete robot with applied human muscle activation patterns for bipedal running," in *Proc. 10th Int. Conf. Humanoid Robots*, 2010, pp. 498–503.
[26] K. Sreenath, H. Park, I. Poulakakis, and J. Grizzle, "A compliant hybrid zero dynamics controller for stable, efficient and fast bipedal walking on mabel," *Int. J. Robot. Res.*, vol. 30, no. 9, pp. 1170–1193, 2011.
[27] K. Radkhah, D. Scholz, O. V. Stryk, M. Maus, and A. Seyfarth, "Towards human-like bipedal locomotion with three-segmented elastic legs," *Proc. 41st Int. Symp. Robot.*, 2010, pp. 1–8.
[28] Y. Blum, H. R. Vejdani, A. V. Birn-Jeffery, C. M. Hubicki, J. W. Hurst, and M. A. Daley, "Swing-leg trajectory of running guinea fowl suggests task-level priority of force regulation rather than disturbance rejection," *PloS one*, vol. 9, no. 6, p. e100399, 2014.
[29] A. Peekema, D. Renjewski, and J. W. Hurst, "Open-source real-time robot operation and control system for highly dynamic, modular machines," in *Proc. ASME 2013, Int. Design Eng. Tech. Conf. Int. Conf. Multibody Syst. Nonlinear Dyn. and Control*, 2013 pp. V07AT10A063 (8 pages).
[30] D. Renjewski, A. Spröwitz, and J. Hurst. (2013). Atrias—A human size compliant bipedal robot walks efficiently. *Proc. Dyn. Walking*. [Online]. Available: http://www.cmu.edu/dynamic-walking/files/abstracts/Renjewski_2013_DW.pdf
[31] H.-K. Shin and B. K. Kim, "Energy-efficient gait planning and control for biped robots utilizing the allowable ZMP region," *IEEE Trans. Robot.*, vol. 30, no. 4, pp. 986–993, Aug. 2014.
[32] K. T. Kalveram and A. Seyfarth, "Inverse biomimetics: How robots can help to verify concepts concerning sensorimotor control of human arm and leg movements," *J. Physiol. Paris*, vol. 103, nos. 3–5, pp. 232–243, 2009.
[33] A. V. Birn-Jeffery, C. Hubicki, Y. Blum, D. Renjewski, J. Hurst, and M. Daley, "Don't break a leg: Running birds from quail to ostrich prioritise leg safety and economy in uneven terrain," *J. Exp. B*, vol. 217, pp. 3786–3796, 2014.